IPP-Report

Max-Planck-Institut für Plasmaphysik

L.M. Shao, E. Wolfrum, G. Birkenmeier, S. Potzel, M. Bernert, M. Cavedon, G.D. Conway, R. Fischer, F.M. Laggner, P. Manz, M. Maraschek, F. Mink, M. Willensdorfer, and the ASDEX Upgrade Team

Oscillating plasma states around the L-H transition at ASDEX Upgrade

IPP 17/51
August, 2016

Oscillating plasma states around the L-H transition at ASDEX Upgrade

L.M. Shao[1,2], E. Wolfrum[1], G. Birkenmeier[1,3], S. Potzel[1], M. Bernert[1], M. Cavedon[1], G.D. Conway[1], R. Fischer[1], F.M. Laggner[4], P. Manz[1,3], M. Maraschek[1], F. Mink[1,3], M. Willensdorfer[1], and the ASDEX Upgrade Team

[1]Max-Planck-Institut für Plasmaphysik, Boltzmannstr. 2, 85748 Garching, Germany
[2]Institute of Plasma Physics, Chinese Academy of Sciences, Hefei 230031, People's Republic of China
[3]Physik-Department E28, Technische Universität München, 85748 Garching, Germany
[4]Institute of Applied Physics, TU Wien, Fusion@ÖAW, Wiedner Hauptstr. 8-10, 1040 Vienna, Austria

August 28, 2016

Abstract

Close to the transition from low to high confinement (L-H transitions), various oscillations at frequencies of a few kilohertz can be observed at ASDEX Upgrade. These oscillations can be of different origin and their differences are illustrated. These oscillations have been identified as the small amplitude limit-cycle oscillations (SALCOs), I-phase and divertor fluctuating detachment state based on characteristics measured with the D-alpha signal, divertor shunt current, magnetic pick-up coils and Absolute eXtreme Ultra Violet (AXUV) diodes. With sufficient auxiliary heating, SALCOs can transit to I-phase. The coexistence of SALCOs and fluctuating detachment state is found before the plasma confinement regime transition. In the paper, the differences between the SALCOs, I-phase and divertor fluctuating detachment state are illustrated.

1 Introduction

During the transition from low to high confinement regimes (L-H transition), a phase with dithering cycles observed by D_α emission or divertor shunt current may appear [1, 2, 3]. This phase named 'intermediate phase' (I-phase) [1] was first introduced by Sanae-I Itoh et. al. at JFT-2M [4]. The I-phase is a phase which emerges in a low density L-mode after raising either the heating power or the density causing the turbulence to rise. A sharp transition is found when the plasma enters the I-phase [1]. Before the L-H transition, limit-cycle oscillations (LCOs) at frequencies of a few kilohertz were observed before the D_α signals or divertor shunt current dropped down in several magnetic devices [5, 6, 7]. This phenomenon was observed mostly before a sharp L-H transition at EAST named 'Small-amplitude LCOs' (SALCOs) [5, 8] and at JFT-2M termed 'Limit-cycle oscillation' [6]. The SALCOs can transit to an I-phase in plasmas with sufficient auxiliary heating [7]. The SALCOs are mostly observed between the L-mode to I-phase transition in ASDEX Upgrade.

Besides the SALCOs and I-phase, a divertor fluctuating detachment state (FS) in the divertor detachment process was observed at ASDEX Upgrade [9, 10, 11]. This state was defined by the appearance of radiative fluctuations with pulsations at around 4-10 kHz, which are situated close to the X-point in the scrape-off layer (SOL). We also know oscillatory phenomena from divertor physics that the targets can oscillate between the onset detachment state and fluctuating detachment state [10]. All the low frequency dithering cycles close to the L-H transition can be measured by a Langmuir probe array at the targets in ASDEX Upgrade.

A predator-prey model (zonal flow and turbulence competition) was proposed to explain the quasi-periodic oscillations in the SALCOs, I-phase and the mechanism of the L-H transition [2, 5, 12, 13, 14]. However, the zonal flows were found to be too weak to trigger the pulses in the SALCOs at JFT-2M [6]. At ASDEX Upgrade the geodesic acoustic mode (GAM) was reported in I-phases [1]. Recent investigation at ASDEX Upgrade shows that the mean flow dominates the shear flow at the plasma edge during the I-phase [15]. Observations from many discharges confirm that the SALCOs to I-phase is a sharp transition with a well-defined threshold, while the full H-mode appears to evolve more softly from the I-phase. The definition of the I-phase seems not very clear, since it does not provide sufficient differences between the I-phase and type-III edge localized modes (ELMs) in H-mode. A former study reported that the magnetic precursor activity is the indicator to distinguish the I-phase and type-III ELMs [16]. A later study at DIII-D showed that the I-phase can smoothly transit to type-III ELMy H-mode [17]. However, a precursor before the dithering burst during I-phase has been observed by radial magnetic pick-up coils [18].

Since these oscillating plasma states close to the L-H transition are similar in phenomenology and probably connect to L-H transition physics, it is necessary to classify them at ASDEX Upgrade. A very convenient and robust way to identify the different oscillation phenomena is the spectral analysis of two types of signals which have a high time resolution and are practically always available: the electromagnetic radiation detected with diodes, and the magnetic signals of pick-up coils. The classification of the above mentioned phenomena by these diagnostics is described in this paper. The paper is organized as follows. Section 2 describes the key diagnostics used in this paper, as magnetic probes and Absolute eXtreme Ultra Violet (AXUV) diagnostic. The differences between the I-phase, SALCOs and divertor fluctuating

state are revealed in section 3. A detailed description of distinguishing the SALCOs and fluctuating detachment state is presented in section 4. The discussion and conclusions are shown in the last section.

2 Magnetic probes and AXUV diagnostic

To distinguish the SALCOs, I-phase and divertor fluctuating detachment state at ASDEX Upgrade, two key diagnostics are used. One is the poloidal and radial magnetic pick-up coils ($\dot{B}_\theta$- and $\dot{B}_r$-coils) and the other is the fast AXUV diodes [19]. A brief introduction to the two diagnostics is presented below.

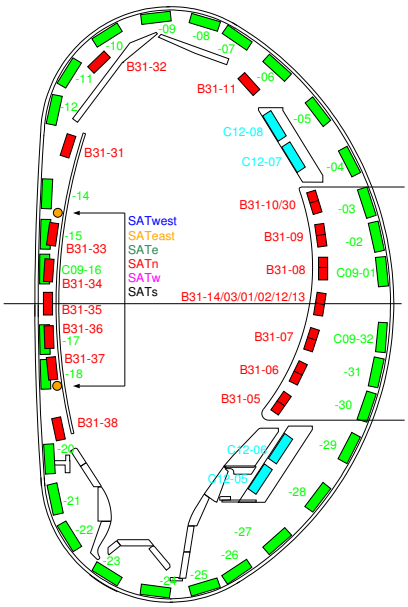

Figure 1: The diagram of poloidal $\dot{B}_\theta$- (C09-X, green) and radial $\dot{B}_r$- (B31-X, red) magnetic pick-up coils in poloidal cross-section.

Figure 1 shows the distribution of the radial ($\dot{B}_r$, red) and poloidal ($\dot{B}_\theta$, green) magnetic pick-up coils at ASDEX Upgrade in the poloidal cross-section. The magnetic probe diagnostics record data with a 2 MHz sampling rate. $\dot{B}_r$-coils have no extension in measurement direction, thus they are sensitive to short wavelengths as expected for filaments in contrast to finite wavelength magnetohydrodynamic activity. Also, due to their high time resolution, they are sensitive to high resonance frequency and proper phase. Moreover, these coils are spread over several low field side and high field side positions as close to the SOL as possible. The 32 $\dot{B}_\theta$-coils cover the whole poloidal cross-section.

A multi-channel photometer system applied for studying fast dynamics of broadband plasma radiation on the microsecond time scale was installed on ASDEX Upgrade since 2008 [20]. Linear arrays of silicon photon diodes, which are encapsulated by pinhole cameras, are utilized for absolute power measurement in the AXUV spectral range. Photons of the vacuum-ultraviolet (VUV) spectral region penetrate the diodes and create electron-hole pairs (n-on-p junction) in the extremely thin passivation layer of the diodes. The spectral

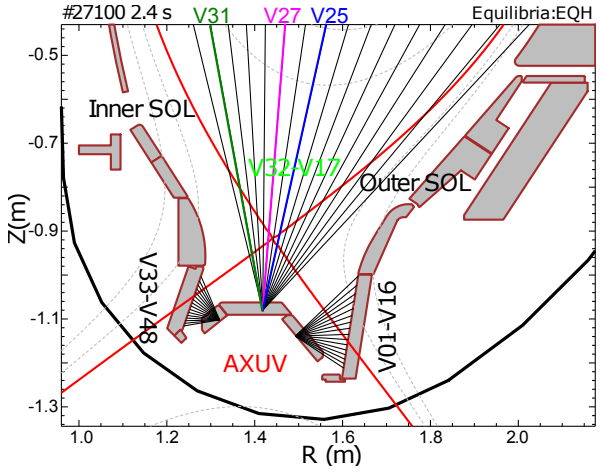

Figure 2: Lines of sight of AXUV diagnostic located at the lower divertor in ASDEX Upgrade. The dark green, magenta and blue lines of sight close to the X-point are channels V31, V27 and V25.

sensitivity covers a wide range of photon energies from the soft X-ray down to the visible part of the spectrum. With the sampling rate up to 500 kHz (applying a 200 kHz low pass Bessel filter on the boards, thus with a time resolution of 5 μs) the AXUV diagnostic enlarges the insights into radiation dynamics of fast plasma phenomena like minor and major disruptions, edge localized modes and divertor detachment process. These are not accessible with usual resistive foil bolometers with the data acquisition rate around 500 Hz [19].

The fast silicon AXUV diode system measures the radiation between 1 eV and 8 keV [20]. This measurement is not absolutely calibrated and has a time resolution of 5 μs. The lines of sight of the diode bolometer at the lower divertor are shown in figure 2. In the lower divertor region, the radiation is mainly emitted with photon energies between 5 and 100 eV. Also the radiation of the plasma in the scrape-off layer is emitted mainly in the VUV region, as a result of the low electron temperature in this region. Inside of the last closed flux surface (LCFS) the electron temperatures are higher than 100 eV, shifting the dominant photon emission to the soft X-ray region ($\sim$100-3000 eV). The chords of V17-V32 above the dome were utilized to classify the divertor detachment process [10]. In this paper, however, channels V27 (magenta line of sight) and V25 (blue line of sight) are mostly used to identify the SALCOs and divertor fluctuating detachment state.

3 Phenomenology of oscillating plasma states

The oscillating phenomena SALCOs and I-phase can appear in a single discharge as shown in the following. Figure 3 shows the temporal evolution of some important plasma parameters of a discharge #29302 with the L-SALCO-I-H transition. The plasma is heated by neutral beam injection (NBI) starting from 3.390 s with plasma current $I_\mathrm{p} = 0.6$ MA, toroidal field $B_\mathrm{T} = -2.5$ T (in clockwise direction) and safety factor $q_{95} = 6.85$. In panel (a), the total net, NBI and Ohmic heating powers as well as the total plasma radiated power including the core and divertor regions are shown. The total net injected power values are obtained from

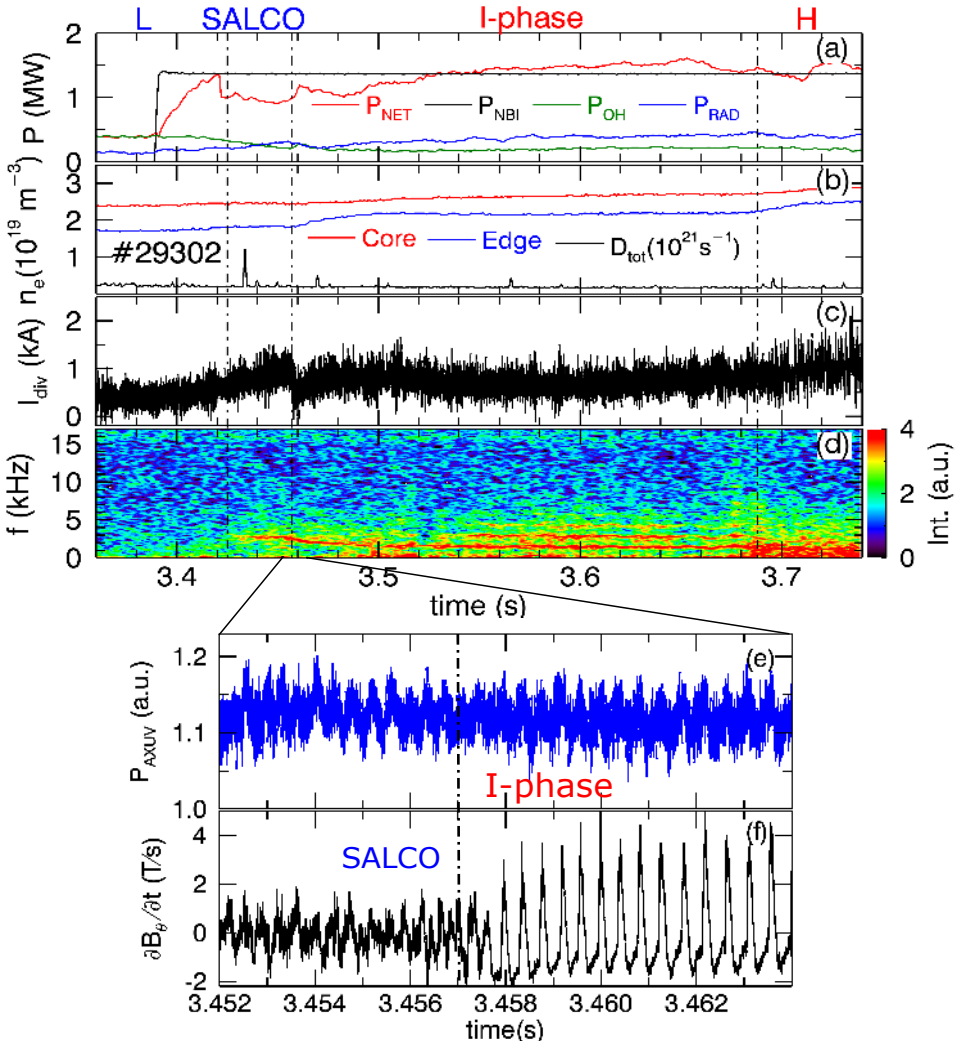

Figure 3: Time evolution of (a) NBI, Ohmic, total net input power and total (core and divertor regions) plasma radiated power, (b) core and edge line-averaged densities as well as deuterium gas fuelling rate, (c) inner divertor shunt current and (d) spectrogram of diode bolometer (AXUV, V31) signal located in the lower divertor of discharge #29302. Panels (e) and (f) show a short segment of the SALCO-I transition in the time slice of 3.452-3.464 s. Raw AXUV signal of channel V31 is shown in (e) and poloidal magnetic pick-up coil measurement (C09-23) is revealed in (f).

the loss power,

$$P_{\mathrm{NET}} = P_{\mathrm{heat}} - dW/dt. \tag{1}$$

Here, P_{heat} is the sum of Ohmic and NBI heating powers subtracted by the loss and unabsorbed parts of injected power, and W is the plasma stored energy. The core and edge electron line-averaged densities ($\bar{n}_{\mathrm{e}}$) as well as the rate of gas fuelling (from the dome) are shown in panel (b). The plasma core and edge line-averaged densities are measured by deuterium cyanide (DCN) interferometer with tangency radii $\rho_{\mathrm{pol}} \approx 0.10$ and $\rho_{\mathrm{pol}} \approx 0.87$, respectively [21]. The plasma enters the I-phase at 3.457 s indicated by a significant drop

of the shunt current measured from the lower inner divertor (I_{div}, see panel (c)) as well as a sharp increase of the plasma edge line-averaged density (see panel (b)). The increased density depends on the neutral gas density in the divertor prior to the L-I transition [22].

Before the plasma enters the I-phase, a SALCOs phase beginning at 3.425 s is observed. With extremely low gas fuelling rate both the core and edge line-averaged densities stay the same in the SALCOs. Although the SALCOs to I-phase transition is a sharp transition, the dithering cycles seem to survive the transition as shown in the spectrogram of AXUV diode (V31, see figure 2) measurement in panel (d) as well as its raw signal (V31) in panel (e). The frequency of dithering cycles decreases from ~ 2.5 to ~ 2.0 kHz when the plasma enters the I-phase from SALCOs. Although the pulses of SALCOS and I-phase are similar in the AXUV diode signals, they are different in the poloidal magnetic measurements located at the lower inner divertor (C09-23, see figure 1) as revealed in panel (f). The poloidal magnetic oscillations in SALCOs become fairly regular spikes when the plasma enters the I-phase. The I-phase transits to H-mode (type-III ELMs phase) at 3.688 s indicated by a fast increased edge line-averaged density shown in panel (b) and irregular pulses measured by the divertor shunt current as well as AXUV diode illustrated in panels (c) and (d).

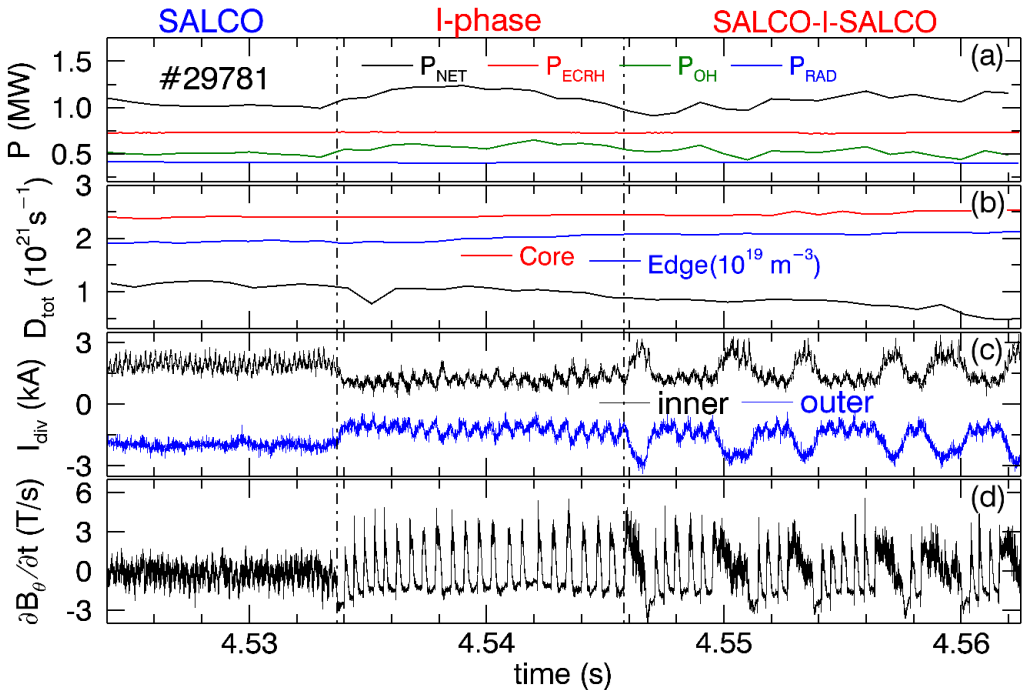

Figure 4: Time evolution of (a) total net, ECRH and Ohmic input power and total plasma radiated power, (b) plasma core and edge line-averaged densities as well as gas fuelling rate, (c) shunt currents from the lower inner as well as outer divertor regions and (d) poloidal magnetic pick-up coil (C09-22) signal of discharge #29781.

As shown in figure 3, the SALCOs can transit to I-phase with sufficient auxiliary heating. However, with really marginal power injection L-I-L [15] and SALCO-I-SALCO oscillations are observed at ASDEX Upgrade. Figure 4 shows the SALCO-I transition as well as SALCO-I-SALCO oscillations in discharge #29781. This discharge is operated with plasma current $I_{\mathrm{p}} = 1.0$ MA, toroidal field $B_{\mathrm{T}} = -2.3$ T and safety factor $q_{95} = 3.85$. In panel (a), the

total net, ECRH (electron cyclotron resonance heating) and Ohmic heating powers as well as the total plasma radiated power including the core and divertor regions are shown. The core and edge line-averaged densities as well as gas fueling rate are shown in panel (b). The shunt currents measured from the lower inner and outer divertor are revealed in panel (c). The plasma enters the I-phase at 4.5337 s and the SALCO-I-SALCO oscillation starts from 4.5458 s. The SALCOs are easier to be observed in the inner divertor shunt current compared to shunt current measured from the outer divertor in this discharge. The poloidal magnetic fluctuation in SALCOs, I-phase as well as SALCO-I-SALCO oscillations are revealed in panel (d). Although the magnetic fluctuation is regular in both SALCOs and I-phase, its amplitude is larger in I-phase than in SALCOs. The SALCO-I-SALCO (as well as L-I-L) oscillations observed at ASDEX Upgrade are irregular at a frequency of a few hundred hertz. The averaged value of magnetic fluctuation is larger in SALCOs, and it declines before the plasma enters the I-phase illustrated in panel (d).

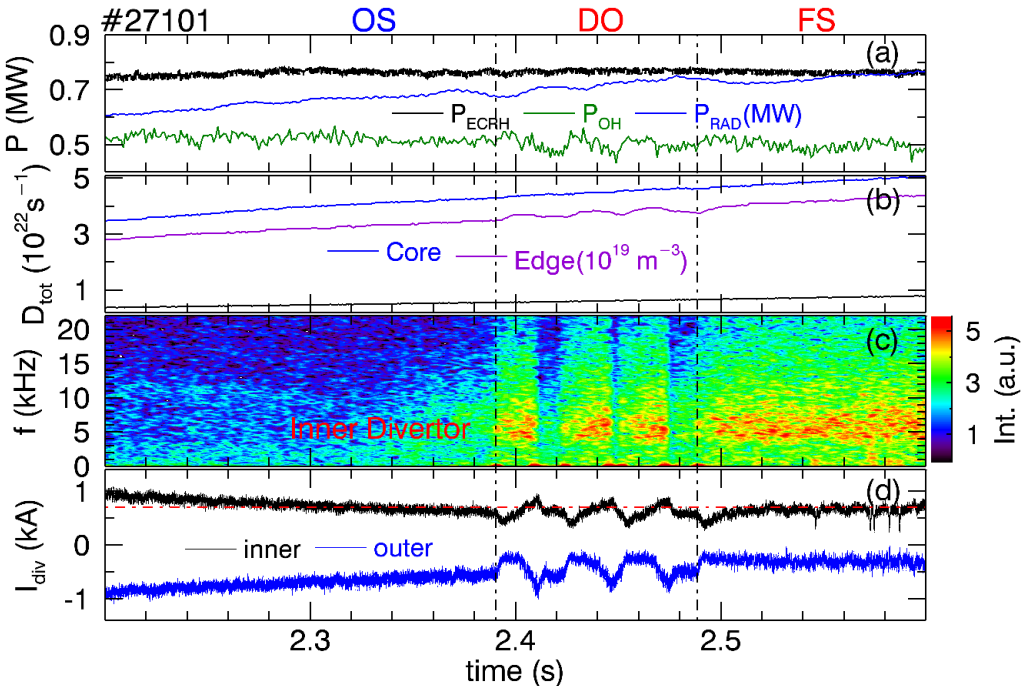

Figure 5: Time evolution of (a) ECRH and Ohmic input power as well as total plasma radiated power, (b) deuterium gas puff rate, core and edge line-averaged densities, (c) spectrogram of diode bolometer (AXUV, V27) signal located at the lower inner divertor and (d) shunt currents measured from the inner and outer lower divertor region of discharge #27101. The divertor oscillation (DO) between onset and fluctuating detachment states from 2.3905 to 2.4885 s is shown. OS and FS are abbreviations for onset divertor detachment and fluctuating divertor detachment state, respectively.

The divertor fluctuating detachment state was observed in the divertor detachment process in both L- and H- mode at ASDEX Upgrade [10, 11, 23]. The whole divertor detachment process can be divided into three states i.e., onset detachment state (OS), fluctuating detachment state (FS) and complete detachment state (CDS) [10]. Figure 5 shows the transition from OS to FS of discharge #27101 with a gas puff ramp. This discharge is operated with

plasma current $I_{\mathrm{p}} = 1.0$ MA, toroidal field $B_{\mathrm{T}} = -2.5$ T and safety factor $q_{95} = 4.09$. In panel (a), the ECRH and Ohmic heating powers as well as the total plasma radiated power including the core and divertor regions are shown. The gas fuelling rate as well as the core and edge line-averaged densities are shown in panel (b). The spectrogram of the AXUV diode measurement on the high field side (V27) of the X-point are revealed in panel (c). The shunt currents measured from the lower inner and outer divertor are illustrated in panel (d).

The broadband spectrum at a frequency of 4-8 kHz is measured by AXUV diodes when the plasma enters the FS. During the OS to FS transition, a divertor oscillation (OS-FS-OS oscillations) is found from 2.3905 to 2.4885 s. The oscillation at frequency of tens of hertz is much less than that of SALCO-I-SALCO oscillation (a few hundred hertz) revealed in panel (c). The edge line-averaged density and shunt currents are also oscillated during the OS-FS-OS oscillations shown in panels (b) and (d). During the OS-FS-OS oscillations, the divertor shunt currents drop as soon as the plasma enters the FS but then increases linearly. When the inner divertor shunt current increases to 0.7 kA (see the horizontal red dashed dotted line), the divertor will return to OS-phase in $\sim$5 ms with the inner shunt current up to $\sim$0.8 kA. With the increase of the gas fueling rate, the divertor enters the stable FS at 2.4885 s with a constant divertor shunt current at 0.7 kA.

Langmuir probe array measurements in the inner divertor and private flux region show that the particle flux oscillates in the same direction in SALCO-I-SALCO oscillations, while evolves oppositely during OS-FS-OS oscillations. Since the SALCO-I-SALCO and OS-FS-OS oscillations appear at separate frequencies of a few hundred and tens of hertz, they can be distinguished easily and we will not discuss them in the details. However, the SALCOs, I-phase and divertor fluctuating detachment state close to the L-H transition at frequencies of a few kilohertz are similar in phenomenology and probably connect to L-H transition physics. The differences between the SALCOs and I-phase are well revealed in figures 3 and 4. It is also not hard to distinguish the I-phase and FS, since the confinement enhancement factor (H-factor) increases when a plasma enters an I-phase while decrease as the divertor enters FS. Nevertheless, the differences between SALCOs and FS are not immediately obvious in L-mode plasmas. Their differences are introduced in next section. All discharges from ASDEX Upgrade analysed in this article are run in the lower single null configuration with the ion ∇B drift towards the active X-point.

4 Differences between SALCOs and FS

As discussed in last section SALCOs, a dithering cycle phase at frequency of a few kilohertz, was mostly observed in low density L-mode discharges with auxiliary heating before the L-H transition. The divertor fluctuating detachment state was observed in the divertor detachment process in both L- and H- mode at ASDEX Upgrade [10, 11, 23]. The similarity between the SALCOs and fluctuating detachment state is that both have particle transport oscillations. Nevertheless, there are a lot of differences between the SALCOs and divertor fluctuating detachment state revealed in the following.

4.1 Difference of SALCOs and FS in AXUV singals

SALCOs and FS can emerge in one L-mode discharge. Figure 6 shows the SALCOs, divertor onset and fluctuating detachment states in a typical gas puff ramp L-mode discharge #27100. The plasma is run with current $I_{\mathrm{p}} = 1$ MA, safety factor $q_{95} = 4.05$ and toroidal field $B_{\mathrm{T}} = -2.5$ T. The plasma is heated by an extremely slow power ramp of ECRH from 0.50-0.55 MW (1.000-2.600 s) as well as a slow power decline of Ohmic heating shown in panel (a). The total net injected power as well as radiated power of the plasma including the core and divertor regions are also shown in panel (a). The plasma stored energy (W_{MHD}) is revealed in panel (b). The core and edge line-averaged densities as well as gas fuelling level stay the same in the SALCOs as shown in panel (c). The gas puff ramp starts at 1.938 s. The oscillations of the SALCOs and FS are illustrated in the spectrogram of the integrated measurements of diode bolometers at high (V27, the magenta line of sight in figure 2) and low (V25, the blue line of sight in figure 2) field sides of the X-point at frequency of a few kilohertz shown in panels (d) and (e). Lower inner divertor shunt current, D_α signal as well as divertor temperature (T_{div}) evaluated from the shunt current [24] are shown in panel (f). T_{div} acts as an indicator for the states of divertor (attachment, partial detachment and complete detachment). The shunt current and divertor temperature increase as soon as the plasma enters the SALCOs, while they decrease with the ramp of the fuelling rate from ∼1.960 s.

The SALCOs happen at low plasma density and low gas fuelling rate, where the edge plasma collisionality is relatively low. With low gas fuelling level both the plasma density and stored energy stay the same in spite of declined Ohmic heating (thus decline of P_{NET}). This suggests that the plasma confinement may increase a bit in the phase of SALCOs. In the lower divertor, the SALCO pulses at a frequency of ∼3.5 kHz are observed by AXUV diodes at both high and low field sides of the X-point. Nevertheless, its amplitude is much stronger at the high field side than that at the low field side of the X-point as shown in panels (d) and (e). The maximum amplitude of the dithering cycles in the SALCOs is located at one of the channels of V29, V30 and V31 (see figure 2). This reveals that the bursts of SALCOs mainly happen at the high field side. The SALCOs do not survive in the divertor onset detachment state at ∼2.020 s shown in panel (d). In panels (d) and (e), the spectrum of the oscillating frequency of 3.5-7 kHz in the divertor fluctuating detachment state is different from the spectrum around 3.5 kHz of the SALCOs. The SALCOs pulses are measured by shunt current and the FS pulses are visible in D_α signal as shown in panel (f). A clear transition from OS to FS at 2.324 s is revealed in panels (d) and (e). The shunt current is higher in the SALCOs compared to FS. In addition, the pulses of the SALCOs are easier identified by shunt current than the pulses in FS. During the SALCOs (1.400-2.020 s), the gas fuelling rate, total plasma radiated power P_{rad}, core and edge line-averaged densities and the plasma stored energy remain the same. P_{rad} as well as the core and edge line-averaged densities increase as soon as the plasma enters the FS shown in panels (a) and (c). In FS, the gas fuelling rate is much higher and the plasma core and edge line-averaged densities increase sharply.

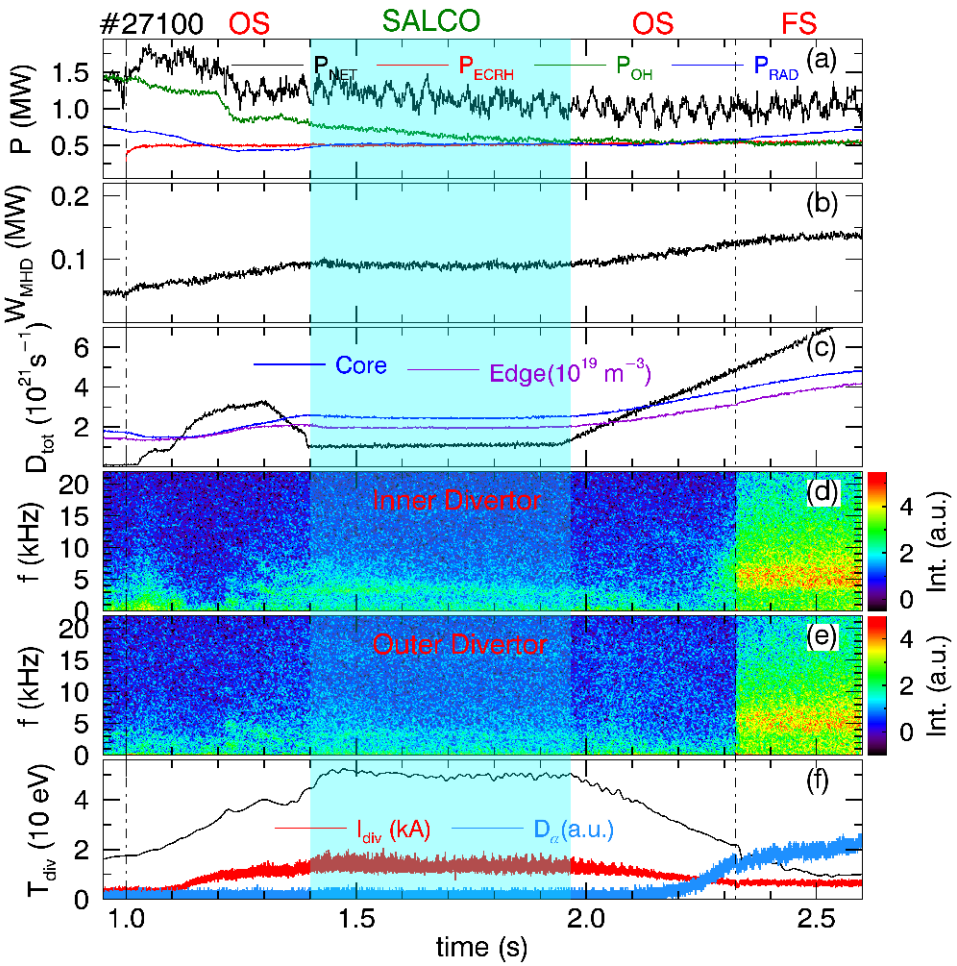

Figure 6: Time evolution of (a) total net, ECRH and Ohmic input power as well as total plasma radiated power, (b) plasma stored energy, (c) deuterium gas puff rate, core and edge line-averaged density, spectrogram of diode bolometer (AXUV) signals located in the (d) inner and (e) outer lower divertor region, (f) lower inner divertor temperature, shunt current and D_α signal.

4.2 Difference of SALCOs and FS in magnetic singals

The dithering cycles of the SALCOs can be observed by both the poloidally and radially separated magnetic pick-up coils. The pulses of the SALCOs are easier to be measured by $\dot{B}_\theta$-coils located behind the upper and lower divertor. Figure 7(a) shows the spectrogram of $\dot{B}_\theta$-coil (C09-22) measurement located just behind the lower inner target (see figure 1) in discharge #27100. The spectrogram is derived with a short-time Fourier transform with a sample window size of $n_{\mathrm{FFT}} = 4096$ and time step length of $n_{\mathrm{step}} = 512$. The ECRH heating was switched on at 1.000 s and after that a magnetic oscillation emerged. The frequency of the magnetic oscillations around 15 kHz was clearly observed in poloidal magnetic probes located at the lower divertor and upper divertor, while they are weaker at inner and outer midplane measured by the poloidal magnetic probes. The magnetic fluctuation of SALCOs started at ∼1.400 s with an oscillating frequency of ∼ 3.5 kHz and its second harmonic as

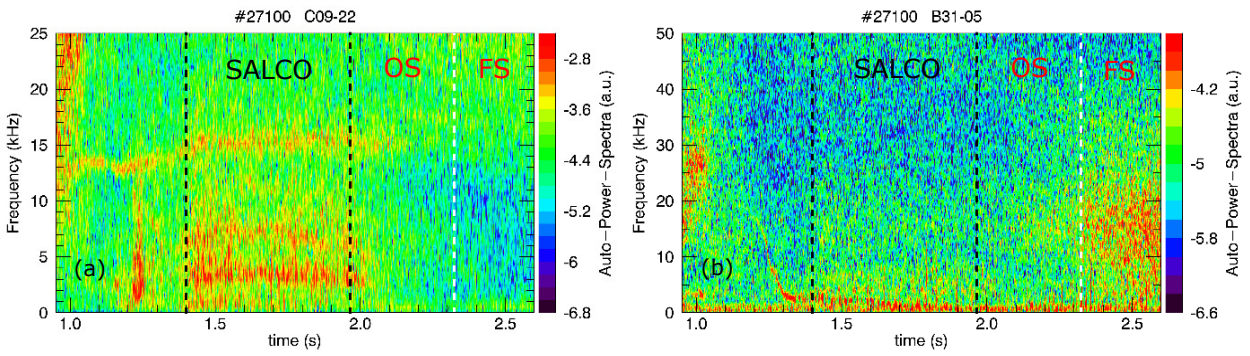

Figure 7: Spectrogram of the measurements of Mirnov coils (a) C09-22 (lower inner divertor) and (b) B31-05 (outer below mid-plane) in discharge #27100.

shown in figure 7(a). The transition between normal L-mode and SALCOs at 1.400 s is indicated by a black dashed line. The frequency of the magnetic oscillations increases from 13 to 15 kHz before the L-mode to SALCOs transition. The $\sim$ 14 kHz oscillation is also measured by AXUV diodes in the inner divertor (1.000-1.400 s). This oscillation could be a GAM due to the frequency range, however the frequency scaling is wrong since the frequency of the oscillation increases although the edge temperature decreases in the same phase. The magnetic oscillations survive after the SALCOs vanish ($\sim$2.020 s) till $\sim$2.120 s when the core line-averaged density increases $\sim$ 25% compared to that in the SALCOs. This suggests that the divertor detachment, corresponding to higher edge collisionality, can kill the SALCOs.

As introduced above, the dithering cycles of SALCOs are measured by the poloidal magnetic probes (see figures 7(a)). The frequency of the SALCOs and its high harmonic is also recognized by the radial magnetic pick-up coils, but is very weak as shown in figure 7(b). The spectrum of the radial magnetic pick-up coil measurements in the SALCOs is quite different from that in I-phase, which has a spike when an I-phase pulse disrupts. The OS and FS transition happens at 2.324 s indicated by the white dashed line shown in figures 7(a) and (b). As soon as the divertor enters the fluctuating detachment state, a magnetic fluctuation with a broadband frequency of 5-25 kHz revealed in figure 7(b) is detected by $\dot{B}_r$-coils located at the low field side (B31-X). However, this magnetic fluctuation cannot be detected by $\dot{B}_\theta$-coils. The relationship between the magnetic fluctuation with a broadband frequency and the fluctuating detachment state at the frequency of 3.5-7 kHz is unclear.

4.3 Coexistence of SALCOs and FS

Figure 6 shows that the SALCOs vanished before the plasma entered the FS. However, the SALCOs and FS always coexist before the L-H transition in 'H-mode standard shot' discharges [25]. Figure 8 shows the temporal evolution of some important plasma parameters of a representative 'H-mode standard shot' discharge #32167 with the detached divertor before the L-I transition. The plasma is heated by NBI blips starting from 1.392 s with plasma current $I_\mathrm{p} = 1$ MA and safety factor $q_{95} = 4.3$. In panel (a), the NBI and Ohmic heating powers as well as the total plasma radiated power including the core and divertor regions are shown. The plasma enters the I-phase at 1.6015 s indicated by a significant drop of D_α signal measured from the lower inner divertor (see panel (b)) as well as a sharp increase

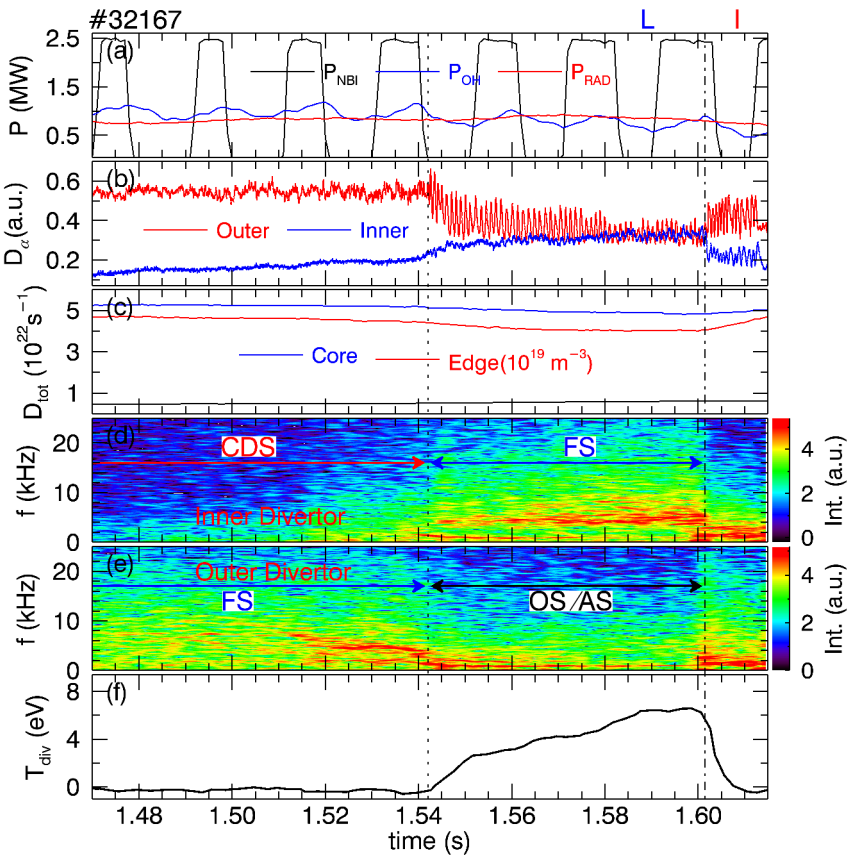

Figure 8: The time trace of (a) NBI and Ohmic heating powers as well as total plasma radiated power, (b) lower inner (red) and outer (blue) divertor D_α signal, (c) gas fuelling rate, core and edge line-averaged densities, (d) spectrogram of AXUV signals in the inner (V28) and (e) outer (V25) divertor and (f) divertor temperature evaluated from shunt current of discharge #32167. The plasma enters the I-phase at 1.6015 s. Legends 'CDS' and 'AS' in (d) and (e) stand for complete detachment state and attachment state of divertor.

of the plasma edge line-averaged density (see panel (c)). The core line-averaged density and rate of gas fuelling (from the dome) controlled by the plasma density feed-back system are revealed in panel (c), either. Before the plasma enters the I-phase, a divertor detachment process over several hundred milliseconds is observed. However, in the divertor detachment process the inner and outer targets can be decoupled and the detachment always starts from the inner target. The divertor being asymmetric, a denser and cooler plasma observed in the inner divertor [26, 27], is the probable reason for the detachment beginning at the inner target.

Before the L-I transition the inner and outer targets behave differently as shown in panels (d) and (e). The complete detachment state (CDS) of the inner divertor is mitigated and returns to the fluctuating state at 1.542 s. The radiative fluctuations in a low kHz-range (∼4 kHz) appearing in the inner scrape-off layer close to the X-point in the fluctuating state are illustrated in the spectrogram of the AXUV integrated signal (V28) in panel (d). In the meanwhile, the fluctuating state of the outer divertor transits to the onset state as well as

attachment state (AS) from 1.542 s as shown in panel (e). As soon as the fluctuating state of the outer target is mitigated and the inner target return to the fluctuating detachment state, the divertor temperature increases shown in panel (f). Moreover, limit-cycle oscillations at a frequency around 1 kHz are observed by D_α signals and AXUV diodes in both inner and outer divertor illustrated in panels (b), (d) and (e). These oscillations are also measured by divertor Langmuir probes and poloidal magnetic pick-up coils at inner and outer targets (not shown here). With the help of these magnetic probe measurements and the AXUV raw signals as well as the analysis in figure 3, the regular pulses at the frequency of $\sim$1 kHz are identified as SALCOs. This analysis shows that the SALCOs and fluctuating detachment state can coexist at the same time.

5 Discussion and conclusions

The dithering cycles at frequencies of a few kilohertz close to L-H transition have been identified as the small-amplitude limit-cycle oscillations (SALCOs), I-phase and divertor fluctuating detachment state (FS) at ASDEX Upgrade. The dithering cycles with regular pulses are observed independently of heating methods (ECRH, NBI or only Ohmic heating). All the low frequency oscillations close to the L-H transition can be measured by D-alpha signal, shunt current, AXUV diodes as well as divertor Langmuir probes at the targets. The SALCOs are observed in L-mode plasmas or before a confinement regime transition. In addition, if there are SALCOs in a L-mode plasma before the plasma confinement regime transition then an I-phase always follows at ASDEX Upgrade. Besides of the kilohertz scale dithering cycles SALCO-I-SALCO oscillations at the frequency of a few hundred hertz as well as divertor OS-FS-OS oscillations around the L-H transition are also observed.

With sufficient auxiliary heating, the plasma in SALCOs can transit to I-phase. Dedicated discharges at ASDEX Upgrade with increased ECRH injected power shot by shot were run at low plasma density, SALCOs were always observed but no transition to I-phase happens although the ECRH heating power increased from 0.32 to 0.90 MW. This means that SALCOs themselves cannot trigger the transition to I-phase. When plasma enters the divertor fluctuating detachment state the edge density gradient becomes steeper, which is beneficial to the L-H transition [28]. The coexistence of SALCOs and FS before the L-I transition are observed in 'H-mode standard shot' discharges. After the plasma transits to I-phase the full H-mode (type-III ELM phase) appears to evolve softly from the I-phase. Thus, the I-phase is more like a part of H-mode [18].

Although these oscillating plasma states close to the L-H transition are similar in phenomenology, they are different in the details as shown in table 1. As mentioned above the SALCO-I-SALCO oscillations at a frequency of a few hundred hertz and the divertor OS-FS-OS oscillations at a frequency of several tens of hertz are much slower than the pulses in SALCOs, I-phase and FS at frequencies of a few kilohertz. Mostly the spectra of the dithering cycles in the SALCOs and I-phase are narrow, while it is a broadband in the fluctuating detachment state. In addtion, both SALCOs and I-phase happen at the plasma edge, and the fluctuating detachment state is measured in the divertor. The SALCO-I-SALCO and OS-FS-OS oscillations are not so regular as the pulses in the SALCOs and I-phase. Except the FS, all fluctuating plasma states can be clearly revealed by divertor shunt currents. The

Table 1: Comparison of oscillating plasma states.

Parameter	SALCOs	I-phase	FS	SALCO-I-SALCO	OS-FS-OS
$f_{\text{oscillations}}$	1-6 kHz	1-6 kHz	4-10 kHz	∼100 Hz	∼10 Hz
spectral feature	narrow	narrow	broad	irregular	irregular
location	edge	edge	divertor	edge	divertor
I_{div}	clear	clear	weak	clear	clear
$\bar{n}_{\text{e}}$	stable	increase	increase	increase	increase
H-factor	stable	increase	decrease	increase	unclear
diagnostics	AXUV/$\dot{B}_\theta$	AXUV/$\dot{B}_\theta$ /$\dot{B}_{\text{r}}$	AXUV/$\dot{B}_{\text{r}}$	$\dot{B}_\theta$	AXUV

plasma density stays the same in SALCOs, while increases in other oscillating plasma states probably. No confinement regime transition is found in SALCOs and the plasma stored energy keeps the same at a low gas fuelling rate. The transition to I-phase is sharp and the increased confinement is observed. The confinement decreases in FS no matter in L- or H- mode. During the SALCO-I-SALCO oscillations the confinement increases compared to the former (or later) L-mode. The variation of the plasma confinement during OS-FS-OS oscillations is not clear.

All pulses of SALCOs, I-phase and FS are measured by AXUV, while their magnetic signals are observed by either or both poloidal and radial magnetic pick-up coils. SALCOs are well detected by poloidal magnetic probes but are very weak in radial magnetic measurements. I-phase pulses are always measured by poloidal and radial magnetic pick-up coils and precursors are visible in a late I-phase or at high plasma density in radial magetic masurements [18]. The oscillating frequency of FS can not be resolved by magnetic probes, while a magnetic fluctuation at a broadband frequency of 5-25 kHz (changed shot by shot) in FS is only measured by radial magnetic probes. SALCO-I-SALCO and OS-FS-OS oscillations are well resolved by poloidal magnetic pick-up coils and AXUV diodes, respectively. With the assistence of the discussion above, the oscillating plasma states around the L-H transition can be conveniently identified or distinguished.

Although the characterisation of the oscillating phenomena can be done quite clearly, the physical origin is mainly unknown. While the I-phase and its physical interpretation was investigated already in references [1, 2, 7, 13, 14, 15, 18, 29], the situation for the SALCOs is different. It can be speculated that the SALCOs are generated by an interaction of zonal-flows with turbulence as already discussed in the context of the I-phase. Other effects like atomic physics in the divertor or unknown states of edge turbulence could be likewise responsible for the SALCO dynamics. The FS was firstly observed at ASDEX Upgrade but the underlying physical mechanism was not fully interpreted [9, 10]. In the pulses of FS the ionization front close to X-point leads to an instability which transports the plasma away, i.e. into the far SOL [10]. Since lack of local radiation and density measurements, we cannot verify whether the oscillations of FS are located at the X-point or in the region between the X-point and strike point (or the far SOL). It will be a subject of the future investigations.

6 Acknowledgments

This work has been carried out within the framework of the EUROfusion Consortium and has received funding from the Euratom research and training programme 2014-2018 under grant agreement No 633053. The views and opinions expressed herein do not necessarily reflect those of the European Commission. L. M. Shao is a fellow of the jointly financed CAS-MPG Doctoral Promotion Programme and F. M. Laggner is a fellow of the Friedrich Schiedel Foundation for Energy Technology.

References

[1] Conway G D, Angioni C, Ryter F, Sauter P, Vicente J, and ASDEX Upgrade Team, Physical Review Letters **106**, 065001 (2011).

[2] Schmitz L, Zeng L, Rhodes T L, Hillesheim J C, Doyle E J, Groebner R J, Peebles W A, Burrell K H, and Wang G, Physical Review Letters **108**, 155002 (2012).

[3] Shao L M, Xu G S, Liu S C, Zweben S J, Wan B N, Guo H Y, Liu A D, Chen R, Cao B, Zhang W, Wang H Q, Wang L, Ding S Y, Yan N, Hu G H, Xiong H, Chen L, Liu Y L, Zhao N, and Li Y L, Plasma Physics and Controlled Fusion **55**, 105006 (2013).

[4] Itoh Sanae-I, Itoh Kimitaka, Fukuyama Atsushi, Miura Yukitoshi, and JFT-2M Group, Physical Review Letters **67**, 2485 (1991).

[5] Xu G S, Wan B N, Guo H Y, Zhao H L, Liu A D, Naulin V, Diamond P H, Tynan G R, Xu M, Chen R, Jiang M, Liu P, Yan N, Zhang W, Wang L, Liu S C, and Ding S Y, Physical Review Letters **107**, 125001 (2010).

[6] Kobayashi T, Itoh K, Ido T, Kamiya K, Itoh S I, Miura Y, Nagashima Y, Fujisawa A, Inagaki S, Ida K, and Hoshino K, Physical Review Letters **111**, 035002 (2013).

[7] Müller S H, Conway G D, Birkenmeier G, Carralero D, Happel T, Herrmann A, Manz P, Marne de P, Mlynek A, Müller H W, Potzel, Rohde V S, Stroth U, Tsalsa M, Tynan G R, Wolfrum E, and ASDEX Upgrade Team, Physics of Plasmas **21**, 042301 (2014).

[8] Xu G S, Wang H Q, Xu M, Wang B N, Guo H Y, Diamond P H, Tynan G R, Chen R, Yan N, Kong D F, Zhao H L, Liu A D, Lan T, Naulin V, Nielsen A H, Juul Rasmussen J, Miki K, Manz P, Zhang W, Wang L, Shao L M, Liu S C, Chen L, Ding S Y, Zhao Nan, Li Y L, Liu Y L, Hu G H, Wu X Q, and Gong X Z, Nuclear Fusion **54**, 103002 (2014).

[9] Potzel S, Wischmeier M, Bernert M, Dux R, Müller H W, Scarabosio A, and the ASDEX Upgrade Team, Journal of Nuclear Materials **438**, S285 (2013).

[10] Potzel S, Wischmeier M, Bernert M, Dux R, Müller H W, Scarabosio A, and the ASDEX Upgrade Team, Nuclear Fusion **54**, 013001 (2014).

[11] Reimold F, Wischmeier M, Bernert M, Potzel S, Kallenbach A, Müller H W, Sieglin B, Stroth U, and the ASDEX Upgrade Team, Nuclear Fusion **55**, 033044 (2015).

[12] Manz P, Xu G S, Wan B N, Wang H Q, Guo H Y, Cziegler I, Fedorczak N, Holland C, Müller S H, Thakur S C, Xu M, Miki K, Diamond P H, and Tynan G R, Physics of Plasmas **19**, 072311 (2012).

[13] Tynan G R, Xu M, Diamond P H, Boedo J A, Cziegler I, Fedorczak N, Manz P, Miki K, Thakur S, Schmitz L, Zeng L, Doyle E J, McKee G M, Yan Z, Xu G S, Wan B N, Wang H Q, Guo H Y, Dong J, Zhao K, Cheng J, Hong W Y, and Yan L W, Nuclear Fusion **53**, 073053 (2013).

[14] Cziegler I, Tynan G R, Diamond P H, Hubbard A E, Hughes J W, Irby J, and Terry J L, Nuclear Fusion **55**, 083007 (2015).

[15] Cavedon M, Pütterich T, Vizzer E, Birkenmeier G, Happel T, Laggner F M, Manz P, Ryter F, Stroth U, and the ASDEX Upgrade Team, Submitted to Nuclear Fusion (2016).

[16] Zohm H, Plasma Physics and Controlled Fusion **38**, 105 (1996).

[17] Colchin R J, Schaffer M J, Carreras B A, McKee G R, Maingi R, Carlstrom T N, Rudakov D L, Greenfield C M, Rhode T L, Doyle E J, Brooks N H, and Austin M E, Physical Review Letters **88**, 255002 (2002).

[18] Birkenmeier G, Cavedon M, Conway G D, Manz P, Stroth U, Fischer R, Fuchert G, Happel T, Laggner F M, Maraschek M, Medvedeva A, Nikolaeva V, Prisiazhniuk D, Pütterich T, Ryter F, Shao L M, Willensdorfer M, Wolfrum E, Zohm H, and the ASDEX Upgrade Team, Nuclear Fusion **56**, 086009 (2016).

[19] Bernert M, Eich T, Burckhart A, Fuchs J C, Giannone L, Kallenbach A, McDermott R M, Sieglin B, and the ASDEX Upgrade Team, Review of Scientific Instruments **85**, 033503 (2014).

[20] Reiter B, Pautasso G, Eich T, Fuchs J C, Giannone L, Dux R, Neuhauser J, Maraschek M, Igochine V, Herrmann A, Lunt T, and the ASDEX Upgrade Team, 36th EPS Conference on Plasma Physics **33E**, P (2009).

[21] Mlynek A, Schramm G, Eixenberger H, Sips G, McCormick K, Zilker M, Behler K, Eheberg J, and ASDEX Upgrade Team, Review of Scientific Instruments **81**, 033507 (2010).

[22] Willensdorfer M, Wolfrum E, Scarabosio A, Aumayr F, Fischer R, Kurzan B, McDermott R M, Mlynek A, Nold B, Rathgeber S K, Rohde V, Ryter F, Sauter P, Viezzer E, and the ASDEX Upgrade Team, Nuclear Fusion **52**, 114026 (2012).

[23] Kallenbach A, Bernert M, Beurskens M, Casali L, Dunne M, Eich T, Guannone L, Herrmann A, Maraschek M, Potzel S, Reimold F, Rohde V, Schweinzer J, Viezzer E, Wischmeier M, and the ASDEX Upgrade Team, Nuclear Fusion **55**, 053026 (2015).

[24] Kallenbach A, Dux R, Fischer R, Geiger B, Giannone L, Herrmann A, Lunt T, Mertens V, McDermott R, Neu R, Pütterich T, Rathgeber S, Rohde V, Schmide K, Schweinzer J, Treutterer W, and the ASDEX Upgrade Team, Plasma Physics and Controlled Fusion **52**, 055002 (2010).

[25] Ryter F, Rathgeber S K, Barrera Orte L, Bernert M, Conway G D, Fischer R, Happel T, Kurzan B, McDermott R M, Scarabosio A, Suttrop W, Viezzer E, Willensdorfer M, Wolfrum E, and the ASDEX Upgrade Team, Nuclear Fusion **53**, 113003 (2013).

[26] Aho-Mantila L, Wischmeier M, Müller H W, Potzel S, Coster D P, Bonnin X, Conway G D, and the ASDEX Upgrade Team, Nuclear Fusion **52**, 103006 (2012).

[27] Chankin A V, Corrigan G, Groth M, Stangeby P C, and JET contributors, Plasma Physics and Controlled Fusion **57**, 095002 (2015).

[28] Shao L M, Wolfrum E, Ryter F, Birkenmeier G, Laggner F M, Viezzer E, Fischer R, Willensdorfer M, Kurzan B, Lunt T, and the ASDEX Upgrade Team, Plasma Physics and Controlled Fusion **58**, 025004 (2016).

[29] Cheng J, Dong J Q, Itoh K, Yan L W, Xu M, Zhao K J, Hong W Y, Huang Z H, Ji X Q, Zhong W L, Yu D L, Itoh S I, Nie L, Kong D F, Lan T, Liu A D, Zou X L, Yang Q W, Ding X T, Duan X R, Liu Ying, and HL-2A Team, Physical Review Letters **110**, 256002 (2013).